

# Adsorption and inhibitive action of hexadecylpyridinium bromide on steel in phosphoric acid produced by dihydrate wet method process

Xiang-Hong Li · Shu-Duan Deng · Hui Fu

Received: 15 April 2010 / Accepted: 4 February 2011 / Published online: 24 February 2011  
© Springer Science+Business Media B.V. 2011

**Abstract** The adsorption and inhibitive action of hexadecylpyridinium bromide (HDPB) on the corrosion of cold rolled steel (CRS) in phosphoric acid produced by dihydrate wet method process (7.0 M H<sub>3</sub>PO<sub>4</sub>) was studied by weight loss, open circuit potential (OCP), potentiodynamic polarization curves, electrochemical impedance spectroscopy (EIS), scanning electron microscope (SEM), and atomic force microscopy (AFM) methods. The results show that HDPB is a good inhibitor in 7.0 M H<sub>3</sub>PO<sub>4</sub>, and its maximum inhibition efficiency (IE) is higher than 90% at little concentrations. The adsorption of HDPB obeys Langmuir adsorption isotherm equation. Thermodynamic parameters (adsorption enthalpy  $\Delta H^0$ , adsorption free energy  $\Delta G^0$ , and adsorption entropy  $\Delta S^0$ ) were calculated and discussed. Polarization curves show that HDPB acts as a mixed-type inhibitor in phosphoric acid. EIS shows that charge-transfer resistance increases with the inhibitor concentration, confirming adsorption process mechanism. The inhibition action of HDPB could also be evidenced by SEM and AFM images. A probable inhibitive mechanism is proposed from the viewpoint of adsorption theory.

**Keywords** Hexadecylpyridinium bromide · Corrosion inhibitor · Phosphoric acid · Wet process · Cold rolled steel · Polarization · EIS · SEM · AFM

## 1 Introduction

The use of inhibitors is one of the most practical methods for protecting materials against corrosion, especially in acidic media [1]. Most well-known acid inhibitors are organic compounds containing nitrogen, sulfur, and oxygen atoms. Among them, the surfactant inhibitor has many advantages such as high inhibition efficiency, low price, low toxicity, and easy production [2]. Surfactants exert their inhibition action through adsorption on the metal surface such that the polar or ionic group (hydrophilic part) attaches to the metal surface while its tail (hydrophobic part) extends to solution. The adsorption of surfactant on metal surface can markedly change the corrosion-resisting property of the metal [3], and so the relationship between adsorption and inhibition is of great importance.

The cationic surfactants of *n*-alkyl-quaternary ammonium salts are considered to be the most effective corrosion inhibitors for iron and steel in hydrochloric and sulfuric acids [4], such as *n*-alkyl quaternary ammonium iodides (C<sub>4</sub>H<sub>9</sub>N(CH<sub>3</sub>)<sub>3</sub>I, C<sub>12</sub>H<sub>25</sub>N(CH<sub>3</sub>)<sub>3</sub>I, and C<sub>16</sub>H<sub>33</sub>N(CH<sub>3</sub>)<sub>3</sub>I) [5], 2-(alkyl (C<sub>n</sub>H<sub>2n+1</sub>) dimethylammonio) alkanol bromides (*n* = 11–15) [6], cetyl benzyl dimethyl ammonium chloride (CBDMAc) [7], 1,2-ethane bis(dimethyl alkyl (C<sub>n</sub>H<sub>2n+1</sub>) ammonium bromide) (*n* = 10, 12, and 16) [8], cetylpyridinium chloride (CPC) [9], hexadecylpyridinium bromide (HDPB), and hexadecyltrimethyl bromide (HDTB) [10]. Generally, the adsorption of *n*-alkyl-quaternary ammonium salts takes place through electrostatic attraction between positively charged –N<sup>+</sup> ion and the

X.-H. Li (✉) · H. Fu  
Department of Fundamental Courses, Southwest Forestry University, Kunming 650224, People's Republic of China  
e-mail: xianghong-li@163.com

S.-D. Deng  
Faculty of Wood Science and Decoration Engineering, Southwest Forestry University, Kunming 650224, People's Republic of China

induced negative charges on metal surface. Furthermore, it has been proposed that heterocyclic systems bearing a quaternized nitrogen atom give better inhibition performance than the alkyl substituted quaternary ammonium compounds [9, 10]. This result can be ascribed to that the chemical adsorption occurs between heterocyclic  $\pi$ -electrons and the empty low-energy d-orbitals of Fe atoms. So, study of the inhibition action of *n*-alkyl-quaternary ammonium compounds on the corrosion of steel is of considerable interest due to its academic and industrial importance. However, no substantial information is available on the corrosion inhibition of quaternary ammonium salts for steel in  $H_3PO_4$  solution.

Phosphoric acid ( $H_3PO_4$ ) is widely used in the production of fertilizers and surface treatment of steel including chemical and electrolytic polishing or etching, chemical coloring, removal of oxide film, phosphating, passivating, and surface cleaning. Most of the acid is produced from phosphate rocks by the so-called dihydrate wet process, equivalent to 7.0 M  $H_3PO_4$  (about 35%  $H_3PO_4$ ) [11]. There is a great need to protect steel materials used in the phosphoric acid industry produced by dihydrate wet method process. However, little work appears to have been done on the corrosion inhibition of steel in 7.0 M  $H_3PO_4$  (or 35%  $H_3PO_4$ ). Jianguo et al. [11] proposed that two polymers of polyvinylpyrrolidone (PVP) and polyethyleimine (PEI) were suitable as corrosion inhibitors for low carbon steel in 7.0 M  $H_3PO_4$ , and inhibition efficiency (IE) values of PVP and PEI were 89 and 90% at 30 °C, respectively. Khamis et al. [12] investigated the corrosion inhibition of steel in 35%  $H_3PO_4$  by some thiosemicarbazide derivatives. Their results showed that the protection efficiency of all the compounds reached up to 99%. Wang [13] reported IE of 2-mercaptopbenzimidazole (MBI) was 75% for mild steel 7.0 M  $H_3PO_4$ . Up to now, literature reveals that data regarding the use of *n*-alkyl-quaternary ammonium salt as corrosion inhibitor for steel in 7.0 M  $H_3PO_4$  is very scarce.

As an ordinary cationic surfactant of *n*-alkyl-quaternary ammonium salt containing pyridinium ring, hexadecylpyridinium bromide (HDPB) has not yet been investigated as an inhibitor for steel in high  $H_3PO_4$  concentration as experienced during production of acid by the so-called dihydrate wet method process. The aim of the present work is to investigate the inhibition effect of hexadecylpyridinium bromide (HDPB) on the corrosion of cold rolled steel (CRS) in 7.0 M  $H_3PO_4$  solution using weight loss, open circuit potential (OCP), potentiodynamic polarization, electrochemical impedance spectroscopy (EIS), scanning electron microscopy (SEM), and atomic force microscopy (AFM) methods. Meanwhile, thermodynamic (adsorption enthalpy  $\Delta H^0$ , adsorption free energy  $\Delta G^0$ , adsorption entropy  $\Delta S^0$ ) are calculated and discussed. A probable mechanism is presented from the viewpoint of adsorption theory.

## 2 Experimental

### 2.1 Materials

Tests were performed on a cold rolled steel (CRS) of the following composition (wt%): 0.07% C, 0.3% Mn, 0.022% P, 0.010% S, 0.01% Si, 0.030% Al, and the remainder Fe.

### 2.2 Inhibitor

The cationic surfactant of hexadecylpyridinium bromide (HDPB) was obtained from Shanghai Chemical Reagent Company of China. Figure 1 shows the molecular structure of HDPB.

### 2.3 Solutions

The aggressive solutions, 7.0 M  $H_3PO_4$  were prepared by dilution of AR grade 85%  $H_3PO_4$  with distilled water. The concentration range of HDPB used is 0.05–1.0 mM.

### 2.4 Weight loss measurements

The cold rolled steel (CRS) sheets of 2.5 cm × 2.0 cm × 0.06 cm were abraded with a series of emery paper (grade 320-500-800) and then washed with distilled water and acetone. After weighing accurately, the specimens were immersed in 250 mL beaker, which contained 250 mL 7.0 M phosphoric acid with different concentrations of HDPB. All the aggressive acid solutions were open to air. After 6 h the specimens were taken out, washed, dried, and weighed accurately. In order to get good reproducibility, experiments were carried out in triplicate. In this study, the standard deviation values among parallel triplicate experiments were found to be smaller than 5%, indicating good reproducibility. The average weight loss of three parallel CRS sheets was obtained. Then the tests were repeated at different temperatures. The temperature was adjusted to ±0.1 °C using a water thermostat. The corrosion rate ( $v$ ) was calculated from the following equation [14]:

$$v = \frac{W}{St} \quad (1)$$

where  $W$  is the average weight loss of three parallel CRS sheets,  $S$  the total area of one CRS specimen, and  $t$  is

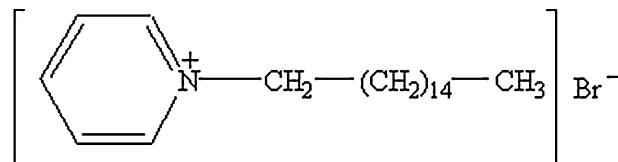


**Fig. 1** Chemical molecular structure of hexadecylpyridinium bromide (HDPB)

immersion time (6 h). With the calculated corrosion rate, the inhibition efficiency ( $IE_w\%$ ) was calculated as follows [14]:

$$IE_w\% = \frac{v_0 - v}{v_0} \times 100 \quad (2)$$

where  $v_0$  and  $v$  are the values of corrosion rate without and with inhibitor, respectively.

## 2.5 Electrochemical measurements

Electrochemical experiments were carried out in a conventional three-electrode cell with a platinum counter electrode (CE) and a saturated calomel electrode (SCE) coupled to a fine Luggin capillary as the reference electrode. To minimize the ohmic contribution, the Luggin capillary was kept close to working electrode (WE). The WE was in the form of a square CRS embedded in PVC holder using epoxy resin so that the flat surface was the only surface in the electrode. The working surface area was  $1.0\text{ cm} \times 1.0\text{ cm}$ , abraded with emery paper (grade 320–500–800), rinsed with distilled water, degreased with acetone, and dried with a cold air stream. Before measurement the electrode was immersed in test solution at open circuit potential (OCP) for 2 h until a steady state was reached. All electrochemical measurements were carried out using PARSTAT 2273 advanced electrochemical system (Princeton Applied Research). Each experiment was repeated at least three times to check the reproducibility.

The potential of potentiodynamic polarization curves was increased at  $0.5\text{ mV s}^{-1}$  and started from a potential of  $-250\text{ mV}$  to  $+250\text{ mV}$  vs. OCP.  $IE_p\%$  is defined as:

$$IE_p\% = \frac{I_{corr} - I_{corr(inh)}}{I_{corr}} \times 100 \quad (3)$$

where  $I_{corr}$  and  $I_{corr(inh)}$  represent corrosion current density values without and with inhibitor, respectively.

Electrochemical impedance spectroscopy (EIS) was carried out at OCP in the frequency range of  $0.01\text{ Hz}$ – $100\text{ kHz}$  using a  $10\text{ mV}$  rms voltage excitation.  $IE_{Rt}\%$  is defined as:

$$IE_{Rt}\% = \frac{R_{t(inh)} - R_{t(0)}}{R_{t(0)}} \times 100 \quad (4)$$

where  $R_{t(0)}$  and  $R_{t(inh)}$  are charge-transfer resistance for CRS in the absence and presence of inhibitor, respectively.

## 2.6 Scanning electron microscopy (SEM) and atomic force microscopy (AFM)

Samples of dimension  $1.5\text{ cm} \times 1.0\text{ cm} \times 0.06\text{ cm}$  were prepared as described above (Sect. 2.4). After immersion in  $7.0\text{ M H}_3\text{PO}_4$  without and with  $1.0\text{ mM HDPB}$  at  $20^\circ\text{C}$

for 6 h, the specimens were thoroughly washed with distilled water, dried with a cold air blaster. SEM and AFM experiments were performed with Japan instrument model (Hitachi High-Tech Science Systems Corporation) S-3000N scanning electron microscope (SEM) and Japan instrument model SPA-400 SPM Unit atomic force microscope (AFM), respectively.

## 3 Results and discussion

### 3.1 Weight loss measurements

#### 3.1.1 Effect of HDPB on corrosion rate

Figure 2 shows the corrosion rate values of CRS in the presence of different concentrations of HDPB in  $7.0\text{ M H}_3\text{PO}_4$  at various temperatures. The corrosion rate value ( $\text{g m}^{-2} \text{h}^{-1}$ ) decreases as HDPB concentration increases, i.e., corrosion inhibition enhances with the inhibitor concentration. This behavior is due to the fact the adsorption amount and coverage of inhibitor on CRS surface increase with the inhibitor concentration [15]. Also, the corrosion rate increases with the temperature both in uninhibited and inhibited solutions. But the corrosion rate increases more rapidly with temperature in the absence of inhibitor. These results confirm that HDPB acts as an efficient inhibitor in the range of temperature studied.

#### 3.1.2 Effect of HDPB on inhibition efficiency

The values of inhibition efficiency obtained from weight loss ( $IE_w\%$ ) for different inhibitor concentrations in  $7.0\text{ M H}_3\text{PO}_4$  are represented in Fig. 3.  $IE_w$  increases as the concentration of inhibitor increases from  $0.1$  to  $1.0\text{ mM}$ .

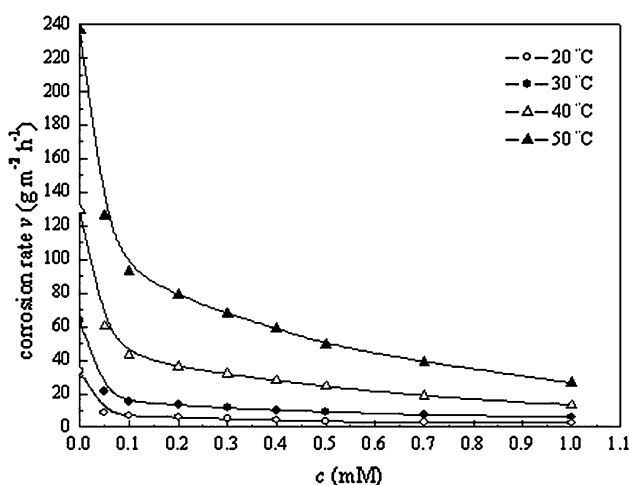


**Fig. 2** Relationship between corrosion rate ( $v$ ) and concentration of HDPB ( $c$ ) in  $7.0\text{ M H}_3\text{PO}_4$

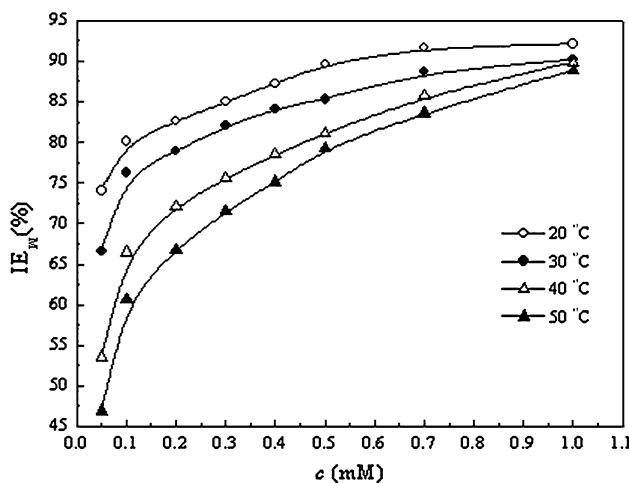


**Fig. 3** Relationship between inhibition efficiency ( $IE_w$ ) and concentration of HDPB ( $c$ ) in 7.0 M  $H_3PO_4$

The maximum  $IE_w$  is about 92.1% at 1.0 mM, and the inhibition is 80% at 20 °C even at very low concentration (0.1 mM), and at 0.5 mM concentration its protection is higher than 90%, which indicates that HDPB is a good inhibitor in 7.0 M  $H_3PO_4$ .

$IE_w$  decreases with an increase in temperature from 20 to 50 °C. The reason can be attributed to that the higher temperatures might cause the desorption of HDPB from steel surface and the corrosion is also increased by the temperature effect on its velocity.

### 3.1.3 Adsorption isotherm

Basic information on interaction between inhibitor and steel surface can be provided by adsorption isotherm. Attempts were made to fit to various isotherms including Frumkin, Langmuir, Temkin, Freundlich, Bockris-Swinkels, and Flory–Huggins isotherms. By far the results are best fitted by Langmuir adsorption isotherm equation [16]:

$$\frac{c}{\theta} = \frac{1}{K} + c \quad (5)$$

where  $c$  is the concentration of inhibitor,  $K$  is the adsorptive equilibrium constant, and  $\theta$  is the surface coverage and calculated by the following equation [16]:

$$\theta = \frac{v_0 - v}{v_0} \quad (6)$$

The linear regressions parameters between  $c/\theta$  and  $c$  are listed in Table 1. Straight lines of  $c/\theta$  vs.  $c$  at different temperatures are shown in Fig. 4. It is observed that all linear correlation coefficients ( $r$ ) are almost equal to 1 and all slopes are close to 1, which indicates the adsorption of HDPB on the steel surface obeys Langmuir adsorption isotherm.

**Table 1** Parameters of the linear regression between  $c/\theta$  and  $c$

Temperature (°C)	Linear correlation coefficient ( $r$ )	Slope	$K (M^{-1})$
20	0.9995	1.06	$4.12 \times 10^4$
30	0.9997	1.08	$3.13 \times 10^4$
40	0.9988	1.06	$1.67 \times 10^4$
50	0.9983	1.06	$1.27 \times 10^4$

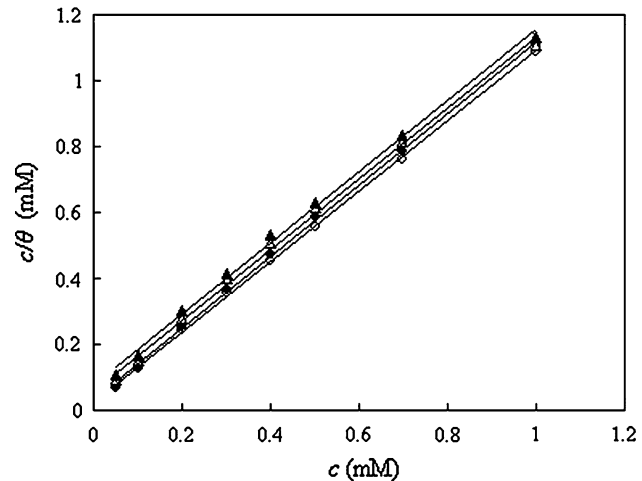


**Fig. 4** The relationship between  $c/\theta$  and  $c$  in 7.0 M  $H_3PO_4$  ○—20 °C; ●—30 °C; △—40 °C; ▲—50 °C

The adsorptive equilibrium constant ( $K$ ) decreases with increasing temperature, which could be attributed to the desorption of inhibitor at higher temperature. In addition, large  $K$  means better inhibition efficiency of a given inhibitor. This is in good agreement with the values of  $IE_w$  obtained from Fig. 3.

### 3.1.4 Thermodynamic parameters

Thermodynamic parameters play an important role in understanding the inhibitive mechanism. The adsorption enthalpy ( $\Delta H$ ) could be calculated according to Van't Hoff equation [14]:

$$\ln K = \frac{-\Delta H}{RT} + \text{constant} \quad (7)$$

where  $R$  is the gas constant ( $8.314 \text{ J K}^{-1} \text{ mol}^{-1}$ ),  $T$  the absolute temperature (K).

Noticeably,  $-\Delta H/R$  is the slope of straight line  $\ln K$  vs.  $1/T$  as shown in Fig. 5. Under experimental conditions, the adsorption enthalpy ( $\Delta H$ ) could be approximately regarded as the standard adsorption heat ( $\Delta H^0$ ) [14, 15]. The standard adsorption free energy ( $\Delta G^0$ ) is obtained according to [17, 18]:

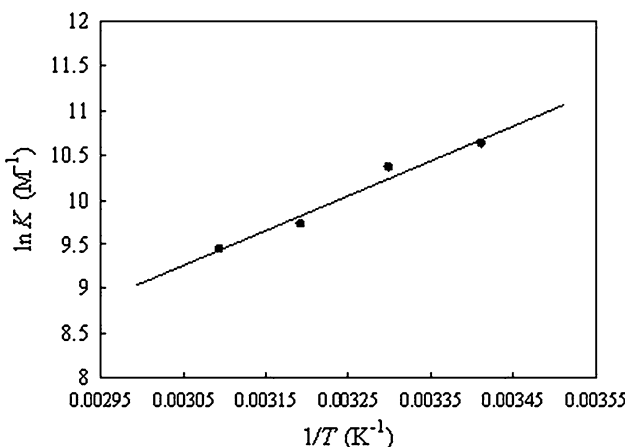


**Fig. 5** The relationship between  $\ln K$  and  $1/T$

$$K = \frac{1}{55.5} \exp\left(\frac{-\Delta G^0}{RT}\right) \quad (8)$$

where the value 55.5 is the concentration of water in solution expressed in M. Then the standard adsorption entropy ( $\Delta S^0$ ) can be obtained by the following thermodynamic basic equation:

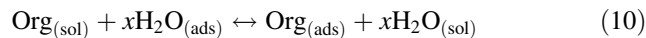
$$\Delta S^0 = \frac{\Delta H^0 - \Delta G^0}{T} \quad (9)$$

All the calculated thermodynamic parameters are listed in Table 2. The negative sign of  $\Delta H^0$  indicates that the adsorption of HDPB is an exothermic process [19], which implies that inhibition performance decreases with increase in temperature. Such behavior can also be interpreted on the basis that increasing temperature resulted in desorption of some adsorbed inhibitor molecules from the metal surface. The negative values of  $\Delta G^0$  indicate that the adsorption of inhibitor molecule onto steel surface is spontaneous. Generally, values of  $\Delta G^0$  up to  $-20 \text{ kJ mol}^{-1}$  are consistent with the electrostatic interaction between the charged molecules and the charged metal (physical adsorption) while those more negative than  $-40 \text{ kJ mol}^{-1}$  involve sharing or transfer of electrons from the inhibitor molecules to the metal surface to form a co-ordinate type of bond (chemisorption) [18, 20, 21]. In this study, the value of  $\Delta G^0$  is  $-35 \text{ kJ mol}^{-1}$ ; probably means that the adsorption involves both physisorption and chemisorption.

**Table 2** Thermodynamic parameters of adsorption of HDPB on the steel surface

Temperature (°C)	$\Delta G^0$ (kJ mol <sup>-1</sup> )	$\Delta H^0$ (kJ mol <sup>-1</sup> )	$\Delta S^0$ (J mol <sup>-1</sup> K <sup>-1</sup> )
20	-35.68	-32.62	10.44
30	-36.22	-32.62	11.88
40	-35.77	-32.62	10.06
50	-36.19	-32.62	11.05

Inspection of Table 2 reveals that the sign of  $\Delta S^0$  is positive. This is opposite to what would be expected, since adsorption is an exothermic process and always accompanied by a decrease of entropy. The reason could be explained as follows: The adsorption of organic inhibitor molecules from the aqueous solution can be regarded as a quasi-substitution process between the organic compound in the aqueous phase [ $\text{Org}_{(\text{sol})}$ ] and water molecules adsorbed on the electrode surface [ $\text{H}_2\text{O}_{(\text{ads})}$ ] [22].



where  $x$  is the size ratio, that is, the number of water molecules replaced by one organic inhibitor. In this situation, the adsorption of HDPB is accompanied by the desorption of water molecules from the surface. So, when the adsorption process for the inhibitor is believed to be associated with a decrease in entropy of the solute, the opposite is true for the solvent. The thermodynamic values obtained are the algebraic sum of the adsorption of organic molecules and desorption of water molecules [23]. Therefore, the gain in entropy is attributed to the increase in solvent entropy and to more positive water desorption entropy [23, 24]. The positive values of  $\Delta S^0$  also means that an increase in disordering takes place in going from reactants to the metal/solution interface [14], which is the driving force for the adsorption of inhibitor onto steel surface [14].

### 3.2 Open circuit potential (OCP) curves

Figure 6 shows the variation of open circuit potential ( $E_{\text{OCP}}$ ) of CRS electrode with time in 7.0 M  $\text{H}_3\text{PO}_4$  solution in the absence and presence of different concentrations of HDPB at 20 °C. In the absence of inhibitor (blank solution), the curve shows a slight increase of  $E_{\text{OCP}}$  towards positive direction followed by small shift in lower

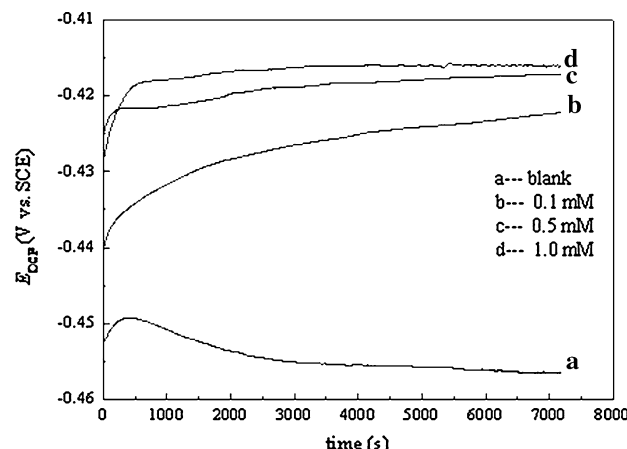


**Fig. 6**  $E_{\text{OCP}}$ —time curves for CRS in 7.0 M  $\text{H}_3\text{PO}_4$  containing HDPB at 20 °C

values of potential. This indicates that the performed oxide layer on the electrode surface dissolves and is not capable to impart passivity to the metal electrode [25]. It takes about 1.5 h to reach the steady state.

On the other hand, curves in the presence of inhibitor exhibit increase in potential towards positive values. The initial potential is moved positive value by time and reaches steady state value after 1.5 h. This indicates that the adsorption of inhibitor molecules on the metal surface and inhibits the corrosion process by stable film formation [26]. It is found that steady state potential moves towards more positive with an increase in HDPB concentration, which implies that the inhibition performance improves with the inhibitor concentration.

### 3.3 Potentiodynamic polarization curves

Potentiodynamic polarization curves for CRS in 7.0 M  $\text{H}_3\text{PO}_4$  with HDPB at 20 °C is shown in Fig. 7. The presence of inhibitor reduces steel corrosion rate, i.e., the anodic curves are moved to more positive potentials, the cathodic curves to more negative potentials, and to lower values of current densities. In other words, both cathodic and anodic reactions of steel electrode corrosion are inhibited by HDPB.

Values of corrosion current densities ( $I_{\text{corr}}$ ), corrosion potential ( $E_{\text{corr}}$ ), cathodic Tafel slope ( $b_c$ ), anodic Tafel

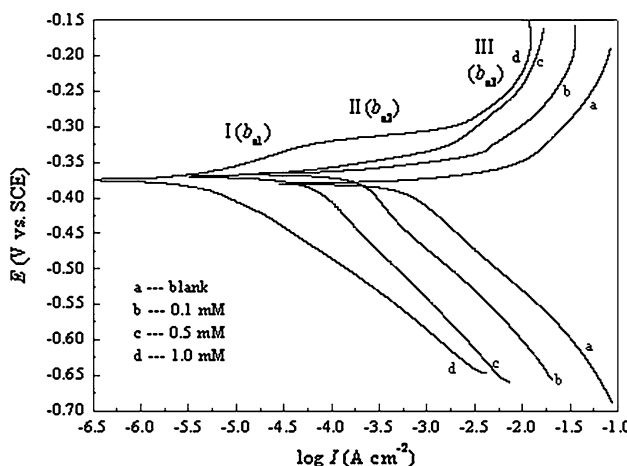


**Fig. 7** Polarization curves for CRS in 7.0 M  $\text{H}_3\text{PO}_4$  containing HDPB at 20 °C

**Table 3** Potentiodynamic polarization parameters for the corrosion of CRS in 7.0 M  $\text{H}_3\text{PO}_4$  containing different concentrations of HDPB at 20 °C

c (mM)	$E_{\text{corr}}$ vs SCE (mV)	$I_{\text{corr}}$ ( $\mu\text{A cm}^{-2}$ )	$-b_c$ ( $\text{mV dec}^{-1}$ )	$b_a$ ( $\text{mV dec}^{-1}$ )	$\text{IE}_p$ (%)
0	-380.5	3682	126	25	—
0.1	-376.9	869	136	23	76.4
0.5	-370.0	497	136	29	86.5
1.0	-375.0	195	85	49	94.7

slope ( $b_a$ ), and inhibition efficiency ( $\text{IE}_p$ ) are listed in Table 3. Clearly,  $I_{\text{corr}}$  decreases prominently while  $\text{IE}_p$  increases with the inhibitor concentration. This trend is in conformity with weight loss data.  $E_{\text{corr}}$  values do not change significantly in inhibited solution as compared to uninhibited solution; therefore, HDPB can be arranged as a mixed-type inhibitor in 7.0 M  $\text{H}_3\text{PO}_4$ , and the inhibition category belongs to the geometric blocking effect [27]. Namely, the inhibition effect comes from the reduction of the reaction area on surface of corroding metal [27, 28]. Tafel slopes of  $b_a$  and  $b_c$  slightly change upon addition of HDPB, suggesting that the HDPB molecules are adsorbed on both anodic and cathodic sites resulting in an inhibition of both anodic dissolution and cathodic reduction reactions.

For anodic polarization with 1.0 mM HDPB, it is worthy noting that three portions (I, II, and III) are observed, which represent the inhibited region, flat region and uninhibited region, respectively. That is, with increase of anodic potentials, the anodic currents increase at a slope of  $b_{a1}$  in portion I. After passing a certain potential, the desorption potential ( $E_{\text{des}}$ ) (about -320 mV vs. SCE), the anodic currents increase steeply and dissolve at a small slope of  $b_{a2}$  in portion II, a flat is observed at this stage. The flat can be attributed to the equilibrium of adsorption and desorption of HDPB molecules on CRS surface [29], and the desorption finishes at the end of this region. The potential value related to the flat is the desorption potential ( $E_{\text{des}}$  vs. SCE), which means the commencement of desorption of the adsorbed species on the electrode surface, above which the coverage of inhibitor decreases rapidly.

For portion III, the anodic current densities change drastically, leading to a sharp increase in Tafel slope of  $b_{a3}$  in the high polarization potential region. The steep increase in current is related to marked desorption of adsorbed inhibitor [30].

### 3.4 Electrochemical impedance spectroscopy (EIS)

Figure 8 shows the Nyquist diagrams for CRS in 7.0 M  $\text{H}_3\text{PO}_4$  at 20 °C containing various concentrations of HDPB. In the absence of inhibitor, the impedance spectra exhibits one single depressed semicircle, this indicates that the charge transfer takes place at electrode/solution interface [31]. In the presence of inhibitor, the impedance spectra consist of large capacitive loop at high frequencies

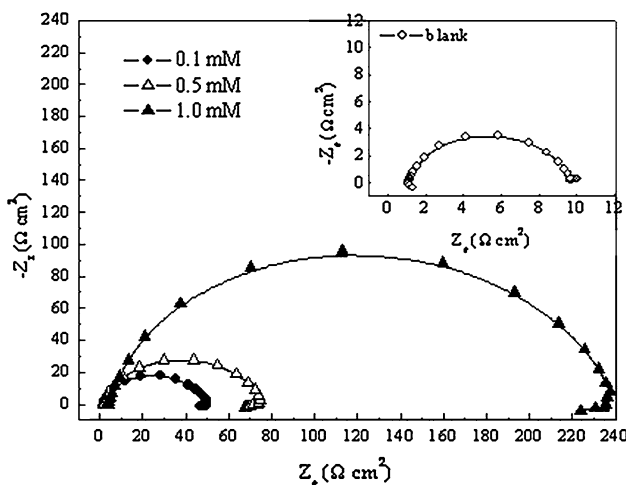


**Fig. 8** EIS of the corrosion of CRS in 7.0 M  $\text{H}_3\text{PO}_4$  with HDPB at 20 °C

followed by a small inductive one at low frequency values. The high frequency capacitive loop is usually related to the charge transfer of the corrosion process and double layer behavior. On the other hand, the low frequency inductive loop in inhibited acid solution may be attributed to the relaxation process obtained by adsorption of inhibitor species [32].

These high frequency capacitive loops are not perfect semicircles which can be attributed to the frequency dispersion as a result of the roughness and inhomogeneous surface of electrode [33]. Furthermore, the diameter of the capacitive loop in the presence of inhibitor is bigger than that in the absence of inhibitor (blank solution) and increases with the inhibitor concentration. This confirms that the impedance of inhibited substrate increases with HDPB concentration.

The EIS results of high frequency capacitive loops are simulated by the equivalent circuit shown in Fig. 9 to pure electric models that could verify or rule out mechanistic models and enable the calculation of numerical values corresponding to the physical and/or chemical properties of the electrochemical system under investigation [34]. The circuit employed allows the identification of both solution resistance ( $R_s$ ) and charge-transfer resistance ( $R_t$ ). It is worth mentioning that the double layer capacitance ( $C_{dl}$ ) value is affected by imperfections of the surface, and that this effect is simulated via a constant phase element (CPE) [35]. The CPE is composed of a component  $Q_{dl}$  and a coefficient  $a$ . The parameter  $a$  quantifies different physical phenomena like surface inhomogeneity resulting from surface roughness, inhibitor adsorption, porous layer formation, etc. The capacitance is deduced from the following relation [36]:

$$C_{dl} = Q_{dl} \times (2\pi f_{max})^{a-1} \quad (11)$$

where  $f_{max}$  represents the frequency at which imaginary value reaches a maximum data on the Nyquist plot. If the electrode surface is homogeneous and plane,  $a$  equals to 1 and the electrode surface can be treated as an ideal capacitance. The value of  $a$  is used to account for the roughness of electrode. The lower is the value of  $a$ , the rougher is the electrode surface. Parametrical adjustment of this circuit with experimental impedance spectra gives access to the double layer capacitance and charge-transfer resistance. The electrochemical parameters of  $R_t$ ,  $f_{max}$ ,  $a$ ,  $C_{dl}$ ,  $IE_{Rt}$ , and respective error % of each parameter are given in Table 4. Error% of each parameter is lower than 5%, which indicates that the proposed model is well representative of high frequency capacitive loops in the investigated system.

In  $\text{H}_3\text{PO}_4$  solutions the value of  $a$  increases in presence of inhibitor on steel surface. For example, the value of  $a$  increases from 0.64 to 0.85 in the presence of 1.0 mM HDPB. These results indicate that the steel surface has become smoother due to formation of a non-porous and dense monolayer of inhibiting film.

In the presence of HDPB,  $R_t$  increases while  $C_{dl}$  decreases with the concentration of HDPB. The decrease in  $C_{dl}$  comparing with that in blank solution (without inhibitor), which can result from a decrease in local dielectric constant and/or

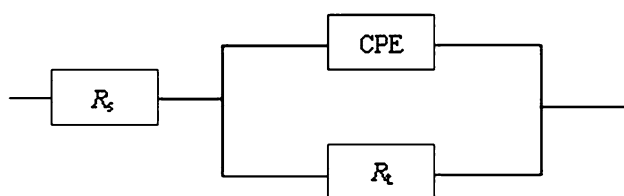


**Fig. 9** The equivalent circuit model of EIS

**Table 4** EIS parameters for the corrosion of CRS in 7.0 M  $\text{H}_3\text{PO}_4$  containing HDPB at 20 °C

$c$ (mM $\text{cm}^{-2}$ )	$R_t$ ( $\Omega \text{ cm}^2$ )	Error of $R_t$ (%)	$a$	Error of $a$ (%)	$f_{max}$ (Hz)	$C_{dl}$ ( $\mu\text{F}$ )	Error of $C_{dl}$ (%)	$IE_{Rt}$ (%)
0	8.7	2.6	0.64	1.3	23.9	759	4.5	–
0.1	49.4	3.1	0.71	1.1	13.7	234	3.8	82.4
0.5	77.3	4.1	0.74	1.9	13.7	150	4.3	88.7
1.0	239.4	2.9	0.85	1.7	7	84	4.6	96.4

an increase in the thickness of the electrical double layer, suggests that the inhibitor molecules function via adsorption at the metal/solution interface [37]. IE<sub>rt</sub> increases with the concentration of HDPB, and reaches to the maximum value 96.4%, which indicates HDPB shows very good corrosion inhibiting behavior for CRS in 7.0 M H<sub>3</sub>PO<sub>4</sub>.

IE obtained from weight loss, potentiodynamic polarization curves and EIS are a little different owing to different conditions of three methods. The difference could be due to the difference in immersion time (the immersion time of polarization and EIS was 2 h, but the weight loss was 6 h) and the discrepancy in the three experimental methods (the weight loss gives average IE, while polarization and EIS give the instantaneous value). But the general rule of IE obtained by three methods is similar. Namely, all three methods indicate that HDPB acts as a good inhibitor for CRS in 7.0 M H<sub>3</sub>PO<sub>4</sub>, and IE increases with the inhibitor concentration.

### 3.5 Scanning electron microscopy (SEM)

Figure 10 shows the SEM images of CRS surface. It can be seen from Fig. 10a that the CRS surface was strongly

damaged after immersion in uninhibited 7.0 M H<sub>3</sub>PO<sub>4</sub>. The corrosion products appear too uneven with many grooves, and the surface layer is extensively rough. In contrast, Fig. 10b shows the formation of thick films on iron surface. In general, the SEM study shows that the inhibited metal surface is smoother than the uninhibited surface. This may be interpreted by the adsorption of inhibitor on CRS surface. It is thought that the molecule of HDPB depresses the corrosion by the formation of a protective film on the steel surface.

### 3.6 Atomic force microscopy (AFM)

The atomic force microscope (AFM) provides a powerful means of characterizing the microstructure [38]. AFM two-dimensional phase images of CRS surface in 7.0 M H<sub>3</sub>PO<sub>4</sub> is presented in Fig. 11. Inspection of Fig. 11a reveals that the CRS surface after immersion in uninhibited 7.0 M H<sub>3</sub>PO<sub>4</sub> (blank) for 6 h shows an aggressive attack of the corroding medium on steel surface, and covered with the corrosion products. It appeared to be relatively uniform in general, and there are no evident black holes or crevices

**Fig. 10** SEM micrographs of CRS surface: (a) after 6 h of immersion at 20 °C in 7.0 M H<sub>3</sub>PO<sub>4</sub>; (b) after 6 h of immersion at 20 °C in 1.0 mM HDPB + 7.0 M H<sub>3</sub>PO<sub>4</sub>

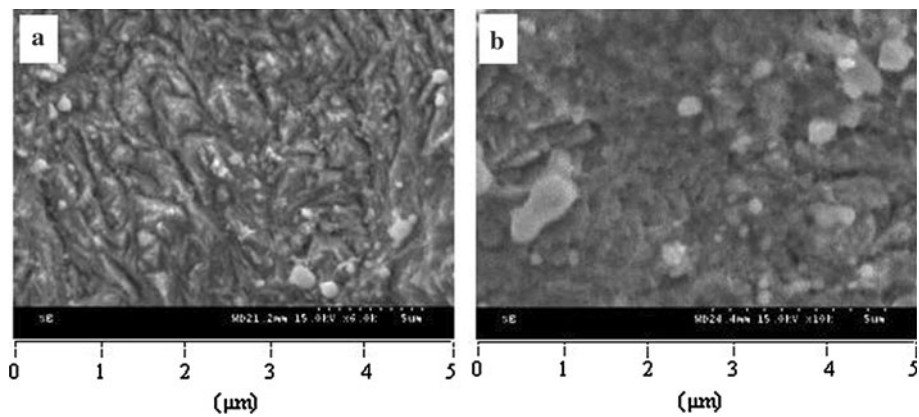


**Fig. 11** AFM two-dimensional phase images of CRS surface: (a) after 6 h of immersion at 20 °C in 7.0 M H<sub>3</sub>PO<sub>4</sub>; (b) after 6 h of immersion at 20 °C in 1.0 mM HDPB + 7.0 M H<sub>3</sub>PO<sub>4</sub>

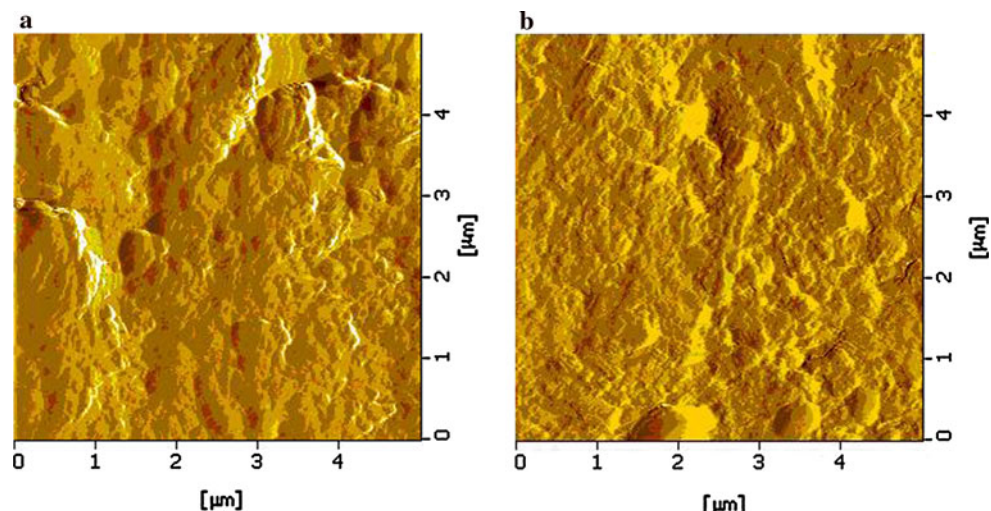
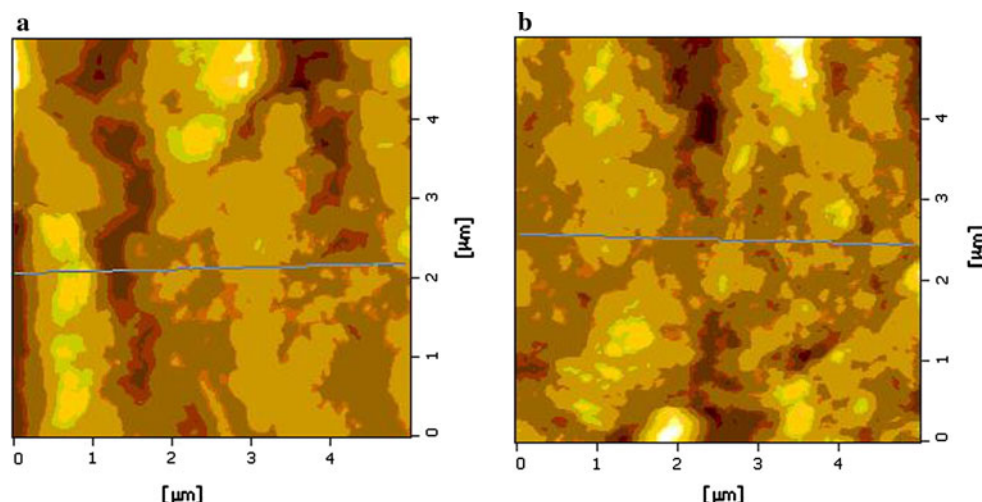


**Fig. 12** AFM topography images of cold rolled steel (CRS) surface (a) after 6 h of immersion at 20 °C in 7.0 M H<sub>3</sub>PO<sub>4</sub>; (b) after 6 h of immersion at 20 °C in 1.0 mM HDPB + 7.0 M H<sub>3</sub>PO<sub>4</sub>



because of the extensive uniform corrosion by acid. Figure 11b shows that the surface is covered with an absorbed layer in the presence of 1.0 mM HDPB. Comparing Fig. 11a with b, it is found that the adsorptive film of inhibitor is different from the corrosion products layer. Therefore, it may be deduced that inhibitor adsorption can effectively protect steel from acid corrosion.

Figure 12 shows the CRS surface topography. As shown in Fig. 12a, the steel surface in uninhibited 7.0 M H<sub>3</sub>PO<sub>4</sub> shows the uneven corrosion products arranging layer upon layer. On the other hand, in the presence of HDPB inhibitor, Fig. 12b appears the relative smaller bunched aggregates distribute across the steel surface, and the inhibitor layer is compact and homogenous.

Figure 13 illustrates the height profiles, which are made along the lines marked in corresponding Fig. 12. Figure 13a indicates that the surface roughness of the CRS after immersion in uninhibited 7.0 M H<sub>3</sub>PO<sub>4</sub> is equal to

363.12 nm, while in the presence of 1.0 mM HDPB, the roughness decreases to 171.19 nm (Fig. 13b). Thus, the roughness is consistent with the results shown in Figs. 11 and 12.

### 3.7 Explanation for inhibition

It has been assumed that organic inhibitor molecule establishes its inhibition action via the adsorption onto the metal surface. The adsorption process is influenced by the chemical structures of the inhibitors, the nature and charged surface of the metal and the distribution of charge over the whole inhibitor molecule. In general, owing to the complex nature of adsorption and inhibition of a given inhibitor, it is impossible for single adsorption mode between inhibitor and metal surface.

The adsorption and inhibition effect of HDPB in H<sub>3</sub>PO<sub>4</sub> solution can be explained as follows: HDPB can be

**Fig. 13** Height profiles of the CRS surface: (a) after 6 h of immersion at 20 °C in 7.0 M H<sub>3</sub>PO<sub>4</sub>; (b) after 6 h of immersion at 20 °C in 1.0 mM HDPB + 7.0 M H<sub>3</sub>PO<sub>4</sub>

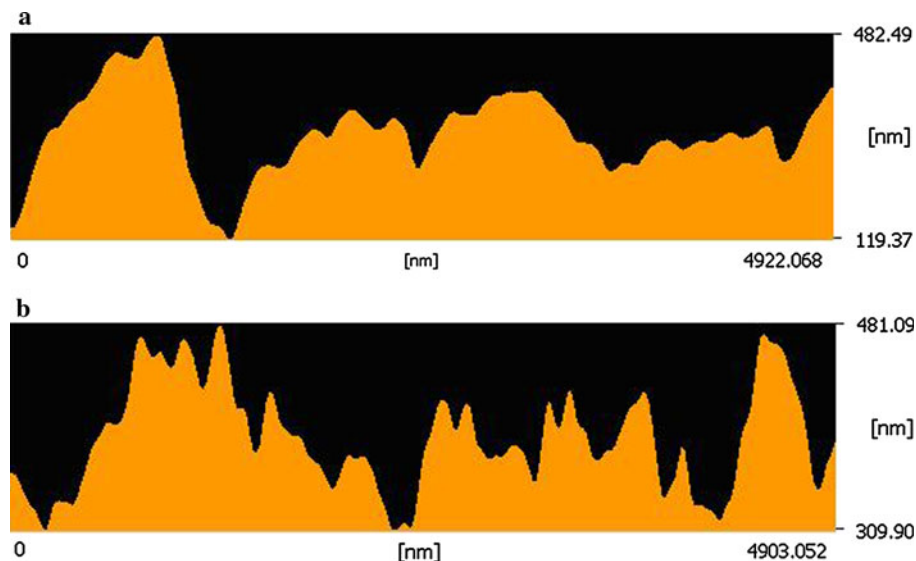
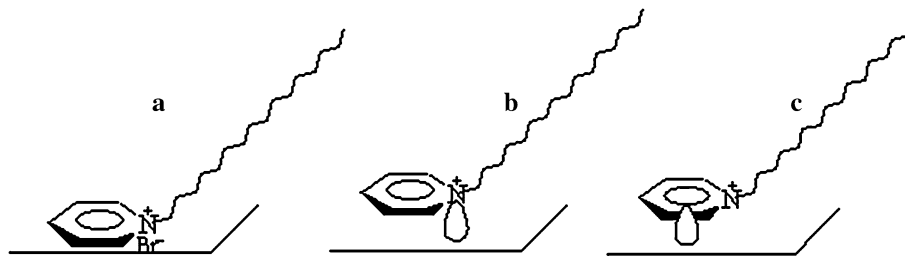


**Fig. 14** Schematic representation of the adsorption mode of HDPB on steel surface: (a) electrostatic attraction between charged  $\text{N}^+$  and  $\text{Br}^-$ ; (b) interaction of unshared electron pairs in N atom with iron surface; (c) interaction between  $\pi$ -electrons of pyridinium ring and vacant d-orbitals of Fe



classified as a 1:1 electrolyte; HDPB is ionized in the acid solution as following:



Thus, HDPB exists the cation organic part ( $[\text{HDP}]^+$ ) and the anion inorganic part ( $\text{Br}^-$ ) in aqueous acidic solutions. Accordingly, HDPB exerts inhibition action by adsorption of  $[\text{HDP}]^+$  on steel surface through that hydrophilic part pyridine ring (the polar or ionic group) attacks the metal surface while the hydrophobic part  $\text{C}_{16}\text{H}_{33}-$  extends to solution face to form a hydrophobic barrier to decrease the corrosion rate. In view of the long hydrocarbon chain length of HDPB ( $\text{C}_{16}\text{H}_{33}-$ ), it is difficult for HDPB adsorb on the steel surface with perpendicular orientation of pyridinium ring. On the other hand, the planar adsorption of pyridinium ring with tilted orientation of alkyl chain ( $\text{C}_{16}\text{H}_{33}-$ ) extending to solution should be more reasonable. This mode of adsorption is shown in Fig. 14. Four types of adsorption may take place in the inhibiting phenomena involving inhibitor molecules at the metal surface as follows:

- (i) Tang et al. [39] reported  $\text{Br}^-$  ions can adsorb on the steel surface in  $\text{H}_3\text{PO}_4$  solution, thus  $[\text{HDP}]^+$  could adsorb through its  $-\text{N}^+$  with adsorbed  $\text{Br}^-$  (Fig. 14a).
- (ii) Owing to lone-pair electrons in N atom, when  $[\text{HDP}]^+$  adsorbed on metal surface, coordinate bond could be formed by partial transference of electrons from the polar atom (N atom) to the metal surface (Fig. 14b).
- (iii) The  $[\text{HDP}]^+$  molecules can be also adsorbed on the metal surface on the basis of donor–acceptor interactions between  $\pi$ -electrons of pyridinium ring and vacant d-orbitals of Fe (Fig. 14c).
- (iv) A combination of the above.

#### 4 Conclusion

- (1) HDPB acts as a good inhibitor for the corrosion of CRS in phosphoric acid produced by dihydrate wet

method process (7.0 M  $\text{H}_3\text{PO}_4$ ). Inhibition efficiency increases with the concentration of the inhibitor, while decreases with the temperature.

- (2) The adsorption of HDPB on CRS surface obeys Langmuir adsorption isotherm. The adsorption process is spontaneous and exothermic and is accompanied by an increase in entropy.
- (3) HDPB acts as a mixed-type inhibitor in 7.0 M  $\text{H}_3\text{PO}_4$ , and the inhibition category belongs to geometric blocking effect. EIS spectra exhibit one capacitive loop in the absence of inhibitor, while in the presence of inhibitor, the impedance spectra consist of large capacitive loop at high frequencies followed by a small inductive one at low frequency values. The addition of HDPB to 7.0 M  $\text{H}_3\text{PO}_4$  solutions enhances  $R_t$  values while reduces  $C_{dl}$  values.
- (4) SEM and AFM images clearly confirm that in the presence of HDPB, the steel surface corrosion is drastically inhibited.

**Acknowledgments** This work was carried out in the frame of research projects funded by Key Construction Course of Chemical Engineering for Forest Products of Southwest Forestry University (XKX200907), and Educational Department of Yunnan Province (09C0181). The electrochemical measurements were carried out on PARSTAT 2273 advanced electrochemical system (Princeton Applied Research) provided by Advanced Science Instrument Sharing Center of Southwest Forestry University.

#### References

1. Trabanelli G (1991) Corrosion 47:410
2. Tizpar A, Ghasemi Z (2006) Appl Surf Sci 252:8630
3. Free ML (2002) Corros Sci 44:2865
4. Niu L, Zhang H, Wei F, Wu S, Cao X, Liu P (2005) Appl Surf Sci 252:1634
5. Schweinsberg DP, Ashworth V (1988) Corros Sci 28:539
6. Elachouri M, Hajji MS, Kerit S, Essassi EM, Salem M, Coudert R (1995) Corros Sci 37:381
7. Vasudevan T, Muralidharan S, Alwarappan S, Iyer SVK (1995) Corros Sci 37:1235
8. Qiu LG, Xie AJ, Shen YH (2005) Corros Sci 47:273
9. Atia AA, Saleh MM (2003) J Appl Electrochem 33:171
10. Saleh MM, Atia AA (2006) J Appl Electrochem 36:899

11. Jianguo Y, Lin W, Otieno-Alego V, Schweinsberg DP (1995) Corros Sci 37:975
12. Khamis E, Ameer MA, AlAndis NM, Al-Senani G (2000) Corrosion 56:127
13. Wang L (2001) Corros Sci 43:2281
14. Li XH, Deng SD, Fu H, Mu GN (2009) J Appl Electrochem 39:1125
15. Zhao TP, Mu GN (1999) Corros Sci 41:1937
16. Li XH, Deng SD, Fu H (2009) Corros Sci 51:1344
17. Cano E, Polo JL, La Iglesia A, Bastidas JM (2004) Adsorption 10:219
18. Li WH, He Q, Zhang ST, Pei CL, Hou BR (2008) J Appl Electrochem 38:289
19. Li XH, Mu GN (2005) Appl Surf Sci 252:1254
20. Bensajay E, Alehyen S, El Achouri M, Kertit S (2003) Anti-Corros Meth Mater 50:402
21. Bentiss F, Lebrini M, Lagrenée M (2005) Corros Sci 47:2915
22. Sahin M, Bilgic S, Yilmaz H (2002) Appl Surf Sci 195:1
23. Branzoi V, Branzoi F, Baibarac M (2000) Mater Chem Phys 65:288
24. Ateya B, El-Anadauli B, El Nizamy F (1984) Corros Sci 24:509
25. Evans UR (1960) Corrosion and oxidation of metals. Edward Arnold, London, p 898
26. Soror TY (2004) J Mater Sci Technol 20:463
27. Cao C (1996) Corros Sci 38:2073
28. Cao CN (2004) Corrosion electrochemistry mechanism. Chemical Industrial Engineering Press, Beijing, p 235 in Chinese
29. Wang J, Cao CN, Chen JJ, Zhang MD, Ye GD, Lin HC (1995) J Chin Soc Corros Prot 15:241 in Chinese
30. Qu Q, Hao ZZ, Li L, Bai W, Liu YJ, Ding ZT (2009) Corros Sci 51:569
31. Larabi L, Harek Y, Traisnel M, Mansri A (2004) J Appl Electrochem 34:833
32. Zhang QB, Hua YX (2010) Mater Chem Phys 119:57
33. Lebrini M, Lagrenée M, Vezin H, Traisnel M, Bentiss F (2007) Corros Sci 49:2254
34. Priya ARS, Muralidharam VS, Subramania A (2008) Corrosion 64:541
35. Bommersbach P, Alemany-Dumont C, Millet JP, Normand B (2006) Electrochim Acta 51:4011
36. Qu Q, Jiang SA, Bai W, Li L (2007) Electrochim Acta 52:6811
37. Lagrenée M, Mernari B, Bouanis M, Traisnel M, Bentiss F (2002) Corros Sci 44:573
38. Gewirth AA, Niece BK (1997) Chem Rev 97:1129
39. Tang LB, Li XM, Liu HC, Mu GN, Liu GH (2006) J Mater Sci 41:1991